10163. Remit in advance $4 for microfiche copy or $7.75 for photocopy. All orders must be prepaid. Institutions and organizations may order by purchase order, but there is a $15 billing and handling charge for this service. For foreign orders, add $4.50 for postage and handling of photocopy or $1.50 for postage of microfiche.
11. S. C. Sevov and J. D. Corbett, in preparation.
12. ______, *Inorg. Chem.* **30**, 4875 (1991).
13. ______, *ibid.* **31**, 1895 (1992).
14. ______, *ibid.* **32**, 1059 (1993).
15. ______, *J. Solid State Chem.* **103**, 114 (1993).
16. ______, *J. Alloys Compd.*, in press.
17. ______, *J. Am. Chem. Soc.*, in press.
18. A. Simon, *Angew. Chem. Int. Ed. Engl.* **27**, 159 (1988).
19. W. B. Pearson, *The Crystal Chemistry and Physics of Metals and Alloys* (Wiley, New York, 1972), pp. 31 and 296.
20. N. N. Greenwood and A. Earnshaw, *Chemistry of the Elements* (Pergamon, Oxford, UK, 1984), p. 171. Only nido (tetrahedral) members Tt_4^{4-}, Tt = Si–Pb and Tr_4^{8-}, Tr = In, Tℓ, are known in "neat" binary systems with alkali metals [H. Schäfer, *Annu. Rev. Mater. Sci.* **15**, 1 (1985); (*15*)].
21. Parameters from C. Janick and R. Hoffmann, *J. Am. Chem. Soc.* **112**, 5924 (1990).
22. A. F. Hebard *et al.*, *Nature* **350**, 600 (1991); K. Holczer *et al.*, *Science* **252**, 1154 (1991); D. W. Murphy *et al.*, *J. Phys. Chem. Solids* **53**, 1321 (1992).
23. Substantially temperature-independent (±20%) susceptibilities lay between −2.6 and −1.2 ($\times 10^{-3}$ electromagnetic units per mole) for the three examples. No superconductivity was evident at 100 Oe and ≥1.4 K.
24. M. M. Alvarez *et al.*, *J. Phys. Chem.* **95**, 10561 (1991).
25. H. Shinohara *et al.*, *Nature* **357**, 52 (1992); C. S. Yannoni *et al.*, *Science* **256**, 1191 (1992).
26. R. Nesper, *Angew. Chem. Int. Ed. Engl.* **30**, 789 (1991); see also the cover of that issue.
27. ______, *Habilitationsschrift* (Universität Stuttgart, Stuttgart, Germany, 1988), p. 166.

28. This research was supported by the U.S. Department of Energy, Office of Basic Energy Sciences, Materials Sciences Division. The Ames Laboratory is operated for the Department of Energy by Iowa State University under contract W-7405-Eng-82.

18 June 1993; accepted 19 August 1993

Crystal Structure of the Polymer Electrolyte Poly(ethylene oxide)$_3$:LiCF$_3$SO$_3$

P. Lightfoot, M. A. Mehta, P. G. Bruce*

Ionically conducting polymers (polymer electrolytes) are under intensive investigation because they form the basis of all solid-state lithium batteries, fuel cells, and electrochromic display devices, as well as being highly novel electrolytes. Little is known about the structures of the many crystalline complexes that form between poly(ethylene oxide) and a wide range of salts. The crystal structure is reported of the archetypal polymer electrolyte poly(ethylene oxide)$_3$:LiCF$_3$SO$_3$, which has been determined from powder x-ray diffraction data. The poly(ethylene oxide) (PEO) chain adopts a helical conformation parallel to the crystallographic *b* axis. The Li$^+$ cation is coordinated by five oxygen atoms—three ether oxygens and one from each of two adjacent CF$_3$SO$_3$$^-$ groups. Each CF$_3$SO$_3$$^-$ in turn bridges two Li$^+$ ions to form chains running parallel to and intertwined with the PEO chain. There are no interchain links between PEO chains, and the electrolyte can be regarded as an infinite columnar coordination complex.

Polymer electrolytes consist of salts, such as LiClO$_4$, that are dissolved in coordinating polymers, such as poly(ethylene oxide) [(CH$_2$CH$_2$O)$_n$]. They can exhibit ionic conductivities approaching that of many liquid electrolytes. Discovered in 1973 by Wright and co-workers (*1*), their potential as completely novel electrolytes with a solid solvent was recognized in 1978 by Armand and co-workers (*2*), who have extensively developed and exploited them. The ability to prepare polymer electrolytes in the form of thin (3 to 30 μm) flexible films of infinite length and with a high ionic conductivity has resulted in the development of a new generation of electrochemical devices with a solid electrolyte and solid electrodes (*3*). Such all-solid-state cells have a number of advantages; they can be fabricated in a wide variety of shapes, the leakage of corrosive liquids is eliminated, and complete devices can be made by automated film processing. Among the devices under development are electrochromic displays, "smart" windows, and rechargeable lithium batteries. The last of these can store large quantities of energy per unit weight and volume. Major investment in the United States, Europe, and Japan is targeted at the development of such batteries for electric vehicle and consumer electronic applications (*4*).

Progress in the field of polymer electrolytes has been severely restricted by the lack of structural data. Part of the difficulty is determining the crystal structures of polymer:salt complexes by single-crystal methods (*5, 6*). We have established the crystal structure of PEO$_3$:NaClO$_4$ (*7*) from high-resolution powder x-ray data. The archetypal polymer electrolyte, LiCF$_3$SO$_3$ dissolved in poly(ethylene oxide), is the most widely investigated system, both for technological applications and fundamental studies. Here we report the elucidation of the crystal structure of the important PEO$_3$:LiCF$_3$SO$_3$ complex from powder x-ray diffraction data (*8*). The use of low-temperature data was critical to the development of a stable structural model through Rietveld refinement. The increase in quality of the high-angle data due to the lowering of thermal motion in such a "soft" molecular system is a significant factor when studying such systems.

Initial indexing of the room-temperature data was carried out with the program

Table 1. Refined atomic parameters for PEO$_3$:LiCF$_3$SO$_3$ at 298 K, space group $P2_1/a$, a = 16.768(2) Å, b = 8.613(1) Å, c = 10.070(1) Å, and β = 121.02(1)°. Hydrogen atoms were included in the refinement but are not reported.

Atom	*x*	*y*	*z*	U_{iso}* (Å^2)
O(1)	0.206(2)	0.110(3)	0.090(3)	0.026(7)
C(1)	0.262(2)	0.091(3)	0.253(3)	0.026(7)
C(2)	0.366(2)	0.099(2)	0.298(2)	0.026(7)
O(2)	0.386(1)	0.246(2)	0.265(2)	0.026(7)
C(3)	0.486(1)	0.261(3)	0.341(3)	0.026(7)
C(4)	0.513(1)	0.426(3)	0.314(2)	0.026(7)
O(3)	0.455(1)	0.469(2)	0.158(2)	0.026(7)
C(5)	0.450(2)	0.631(2)	0.131(3)	0.026(7)
C(6)	0.387(2)	0.651(3)	−0.051(4)	0.026(7)
S(1)	0.2697(7)	0.124(2)	0.809(1)	0.084(9)
C(7)	0.328(1)	0.077(2)	0.703(2)	0.084(9)
O(4)	0.277(2)	−0.001(2)	0.903(2)	0.11(1)
O(5)	0.303(2)	0.264(2)	0.893(3)	0.11(1)
O(6)	0.172(1)	0.150(4)	0.693(2)	0.11(1)
F(1)	0.321(2)	0.204(2)	0.624(3)	0.24(1)
F(2)	0.284(2)	−0.031(2)	0.601(3)	0.24(1)
F(3)	0.413(1)	0.041(3)	0.798(2)	0.24(1)
Li(1)	0.156(5)	0.903(11)	0.906(9)	0.05

*Values constrained according to atom type. Li not refined.

Centre for Electrochemical and Materials Sciences (CEMS), Department of Chemistry, University of St. Andrews, St. Andrews, Fife, Scotland, KY169ST, United Kingdom.

*To whom correspondence should be addressed.

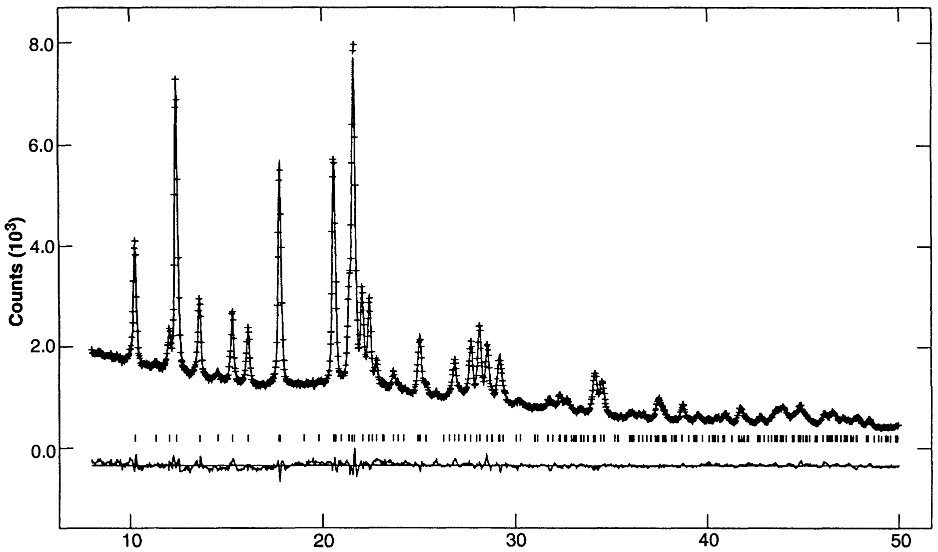

Fig. 1. Final observed (plus marks), calculated (solid line), and difference profiles (below) for the Rietveld refinement of PEO_3:$LiCF_3SO_3$ at 298 K.

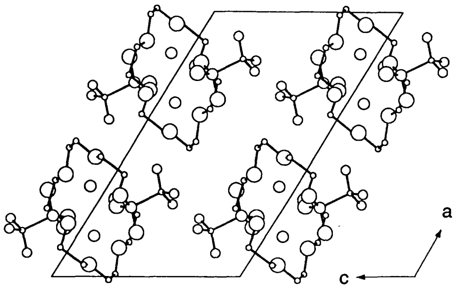

Fig. 2. View of the PEO_3:$LiCF_3SO_3$ structure along the chain axis (*b*).

TREOR (*9*). The first 20 observable lines were indexed to give a monoclinic cell a = 10.064 Å, b = 8.613 Å, c = 14.441 Å, and β = 95.65°, space group $P2_1/n$. This cell can be transformed to the alternative setting in $P2_1/a$: a = 16.77 Å, b = 8.613 Å, c = 10.064 Å, and β = 121.0°, which bears a resemblance to Chatani's cell for the PEO_3:NaSCN complex (*6*) (a = 16.83 Å, b = 7.19 Å, c = 10.64 Å, and β = 125.5°). On this basis, the structure of PEO_3:NaSCN was used to provide a partial starting model for the Rietveld refinement of the present structure, by initially using our 100 K data (*10*). Preliminary refinement then involved least-squares minimization of this partial model against the powder diffraction pattern, but limited to the range of bond distances and angles specified by the constraints, with the program GSAS (*11*). At this stage the fit to the raw diffraction data was sufficiently good to allow successive difference Fourier techniques to be applied with Rietveld refinement in order to determine the remainder of the structure (specifically, the location of the $CF_3SO_3^-$ moiety), with soft constraints again being added to stabilize the geometry of the $CF_3SO_3^-$ group as the model was developed [S–C = 1.82(1) Å, S–O = 1.42(1) Å, C–F = 1.32(1) Å, and tetrahedral angles of 109°]. The soft constraints effectively act as additional observations, which were necessary to improve the data-to-parameter ratio and thus stabilize the refinement of such a complex structure from relatively poor powder diffraction data. The position of the Li^+ ion was determined geometrically at a point within the PEO chain with distances from the oxygens that are typical for Li^+–O coordination and then was allowed to refine freely. This procedure significantly improved the profile fit and yielded a simple geometry around the Li^+ position (see below). Attempts to refine the Li^+ ion in other positions were unsuccessful. In the final refinement cycles, isotropic temperature factors U_{iso} were given to all atoms, and these were grouped according to atom type (see Table 1). The temperature factors for Li and H were not refined.

The large values of U_{iso} for the atoms in the $CF_3SO_3^-$ group may suggest one of three possibilities: (i) a site occupancy less than unity; (ii) dynamic (thermal) disorder of the CF_3SO_3 group; and (iii) static (positional) disorder. Our model naturally requires a stoichiometry PEO_3:$LiCF_3SO_3$, in agreement

Table 2. Selected bond lengths and angles.

Atoms	Distance (Å)	Atoms	Angle (degree)
O1–C1	1.42(1)	C6–O1–C1	108(1)
C1–C2	1.56(1)	O1–C1–C2	108(1)
C2–O2	1.40(1)	C1–C2–O2	110(1)
O2–C3	1.45(1)	C2–O2–C3	109(1)
C3–C4	1.55(1)	O2–C3–C4	111(1)
C4–O3	1.41(1)	C3–C4–O3	110(1)
O3–C5	1.41(1)	C4–O3–C5	115(1)
C5–C6	1.58(1)	O3–C5–C6	105(1)
C6–O1*	1.44(1)	C5–C6–O1*	106(1)
S1–O4	1.39(1)	O1–Li1–O2	174(5)
S1–O5	1.42(1)	O1–Li1–O3	85(3)
S1–O6	1.46(1)	O1–Li1–O4	77(3)
S1–C7	1.83(1)	O1–Li1–O5	83(3)
C7–F1	1.31(1)	O2–Li1–O3	94(4)
C7–F2	1.30(1)	O2–Li1–O4	99(3)
C7–F3	1.28(1)	O2–Li1–O5	104(4)
Li1–O1	2.38(9)	O3–Li1–O4	134(5)
Li1–O2	2.01(8)	O3–Li1–O5	107(4)
Li1–O3	1.72(7)	O4–Li1–O5	112(4)
Li1–O4	2.21(8)		
Li1–O5	2.14(8)		

*Symmetry operator: (i) 1/2 − *x*, 1/2 + *y*, − *z*.

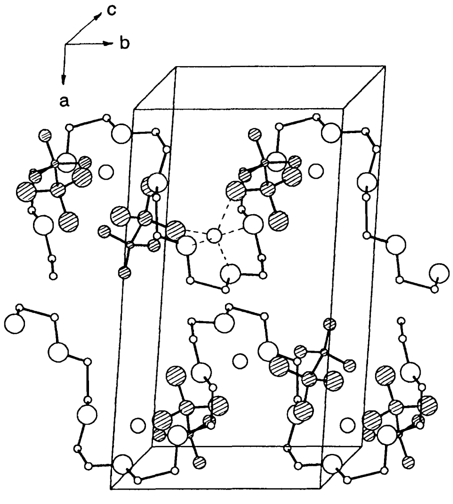

Fig. 3. View of the structure along *c*. $CF_3SO_3^-$ groups are shaded. For clarity, coordination around one Li^+ is shown in dashed lines.

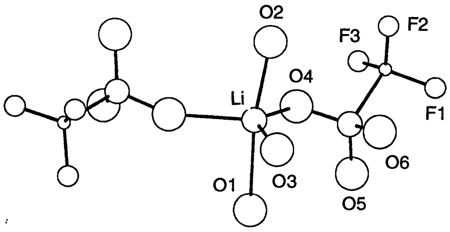

Fig. 4. Local environment around Li$^+$, showing coordination by three ether oxygens and oxygens from two neighboring triflate groups.

with the phase diagram study of Vallée, Besner, and Prud'homme (*12*). Several earlier reports have suggested stoichiometries of PEO$_4$:LiCF$_3$SO$_3$ or PEO$_{3.5}$:LiCF$_3$SO$_3$ (*13*). This would require partial occupancy of the Li/CF$_3$SO$_3$ sites in our model. In order to explore the stoichiometry, we fixed the temperature factors for the Li/CF$_3$SO$_3$ species at 0.08 Å^2. After refinement, the occupancy value was 0.96(1), which sets an upper limit on the PEO:LiCF$_3$SO$_3$ ratio of 3.13(3). We can reasonably conclude that there is no significant deviation from the ideal 3:1 stoichiometry. The latter two possible explanations for the high thermal parameters were explored by carrying out low-temperature refinements. The relatively smooth variation of U_{iso} versus temperature observed for F and O suggests that this phenomenon is associated merely with thermal and not static disorder. The relatively large displacements (0.10 Å) for F even at low temperature are not surprising and may be expected from the very weak coordination of this part of the complex.

Results of the Rietveld refinement for the room-temperature structure are given in Tables 1 and 2. The final model consisted of 113 variables refined against 2600 data points and 88 soft constraints. The data range covered was $8° < 2\theta < 60°$ (Fig. 1). Final agreement factors were $R_{wp} = 3.84\%$ and $\chi^2 = 1.83$. Views of the structure along *b* and *c* are given in Figs. 2 and 3, respectively. The helical arrangement of the PEO chain within the unit cell is similar to that for the previously determined 3:1 complexes, NaSCN (*5*), NaI (*6*), and NaClO$_4$ (*7*). However, the disposition of the inorganic portion of the structure relative to this is significantly different than in the previous cases, reflecting the different size and shape of the anion and the smaller size of the cation. Focusing on one PEO chain (Figs. 2 and 3), the Li$^+$ ions are located within it, forming a zigzag pattern along the axis of the helix (that is, *b*). Lithium is coordinated by five oxygens, composed of three PEO oxygens and one oxygen from each of two different CF$_3$SO$_3^-$ groups (Figs. 3 and 4). The coordination is best described as trigonal bipyramidal, with the three PEO oxygens being almost coplanar. Each CF$_3$SO$_3^-$ group associated with the chain bridges two adjacent Li$^+$ ions, one oxygen being coordinated to each lithium, leaving the third oxygen free. There is little interchain interaction, the –CF$_3$ groups being located in the space between the chains. The crystal structure demonstrates strikingly that these compounds are columnar coordination complexes, with long chains of Li$^+$ ions being coordinated by ether oxygens and triflate anions (Fig. 2), the solid polymer results from chain entanglement rather than any ionic cross-linking. It is also evident from the crystal structure that replacement of the –CF$_3$ group with a bulkier, preferably asymmetric group, would inhibit crystallization. This is presumably the origin of the wide range of amorphicity exhibited by PEO:Li[(CF$_3$SO$_2$)$_2$N] and PEO:Li[(CF$_3$SO$_2$)$_3$C].

REFERENCES AND NOTES

1. D. E. Fenton, J. M. Parker, P. V. Wright, *Polymer* **14**, 589 (1973).
2. M. B. Armand, J. M. Chabagno, M. Duclot, in *Fast Ion Transport in Solids*, P. Vashista, J. M. Mundy, G. K. Shenoy, Eds. (North-Holland, Amsterdam, 1979), p. 131.
3. J. R. MacCallum and C. A. Vincent, Eds., *Polymer Electrolyte Reviews* (Elsevier, London, 1989), vols. 1 and 2.
4. F. M. Gray, *Solid Polymer Electrolytes: Fundamentals and Technological Applications* (VCH Press, Cambridge, United Kingdom, 1991).
5. Y. Chatani and S. Okamura, *Polymer* **28**, 1815 (1987).
6. Y. Chatani, Y. Fujii, T. Takayanagi, A. Honma, *ibid.* **31**, 2238 (1990).
7. P. Lightfoot, M. A. Mehta, P. G. Bruce, *J. Mater. Chem.* **2**, 379 (1992).
8. Powder x-ray diffraction data were collected on a Stoe STADI/P system (equipped with a position-sensitive detector covering ~6° in 2θ) with monochromatized CuK$_{\alpha1}$ radiation. The sample was mounted in a 0.5-mm Lindemann tube, and data were collected over the range $8° < 2\theta < 60°$ and at temperatures between 100 and 298 K. Low-temperature runs were performed with an Oxford Cryostream system.
9. P.-E. Werner, *Z. Kristallogr.* **120**, 375 (1964).
10. Coordinates for the PEO part of the structure were used directly from Chatani's refinement, with the addition of hydrogen atoms in idealized positions. Because of the differing cell size, the coordinates of the atoms in the chain had to be adjusted to produce an idealized PEO chain conforming to the known "*trans-trans-gauche*" conformation (*5*). Soft (chemical) constraints on both bond lengths and angles were used in order to optimize this geometry, namely C–O = 1.44(1) Å, C–C = 1.57(1) Å, and C–H = 1.09(1) Å (errors in the last digit given in parentheses), with tetrahedral angles at 109° and C–C and C–O torsion angles at 60° and 180°, respectively.
11. A. C. Larson and R. B. Von Dreele, *Los Alamos Natl. Lab. Rep. No. LA-UR-86-748* (1987).
12. A. Vallée, S. Besner, J. Prud'homme, *Electrochim. Acta* **37**, 1579 (1982).
13. P. R. Sorensen and T. Jacobsen, *Polym. Bull.* **9**, 47 (1983); C. Berthier *et al.*, *Solid State Ionics* **11**, 91 (1983).
14. P.G.B. is indebted to the Royal Society for the award of a Pickering Research Fellowship and to SERC for financial support.

7 June 1993; accepted 7 September 1993

Fire History and Climate Change in Giant Sequoia Groves

Thomas W. Swetnam

Fire scars in giant sequoia [*Sequoiadendron giganteum* (Lindley) Buchholz] were used to reconstruct the spatial and temporal pattern of surface fires that burned episodically through five groves during the past 2000 years. Comparisons with independent dendroclimatic reconstructions indicate that regionally synchronous fire occurrence was inversely related to yearly fluctuations in precipitation and directly related to decadal-to-centennial variations in temperature. Frequent small fires occurred during a warm period from about A.D. 1000 to 1300, and less frequent but more widespread fires occurred during cooler periods from about A.D. 500 to 1000 and after A.D. 1300. Regionally synchronous fire histories demonstrate the importance of climate in maintaining nonequilibrium conditions.

Despite the complexity inherent in local fire regimes, regional fire activity often oscillates in phase with year-to-year climatic variability. For example, the area burned annually across the southern United States tends to decrease during El Niño years and increase during La Niña years (*1*). This coupling between wildland fire and climate raises the possibility that intrinsic and stochastic factors, while contributing to local ecosystem heterogeneity, are overridden by regional climatic events and trends. Rapid, regional changes in vegetation may result from extreme climate-linked disturbances, such as catastrophic crown fires, whereas relatively slow vegetation changes may follow gradual, climate-driven shifts in surface-fire regimes (*2*). A broad range of spatial and temporal observations is therefore necessary to distinguish local- from regional-scale patterns and to encompass both high- and low-frequency changes in processes (*3*).

A commonly observed but rarely quantified phenomenon of disturbance regimes is

---

Laboratory of Tree-Ring Research, University of Arizona, Tucson, AZ 85721.